The Bauschinger Effect on 3-D SIFs for Networks of Radial and Longitudinally-Coplanar Semi-Elliptical Internal Surface Cracks In Autofrettaged Pressurized Thick-Walled Cylinders

Q. Ma[1], C. Levy[2] and M. Perl[3]

Abstract: Networks of radial and longitudinally-coplanar, internal, surface cracks are typical in rifled, autofrettaged, gun barrels. In two previous papers, the separate effects of large arrays of either radial or longitudinally-coplanar semi-elliptical, internal, surface cracks in a thick-walled, cylindrical, pressure vessel under both ideal and realistic autofrettage were studied. When pressure is considered solely, radial crack density and longitudinal crack spacing were found to have opposing effects on the prevailing stress intensity factor, K_{IP}. Furthermore, the addition of the negative stress intensity factor (SIF), K_{IA}, resulting from the residual stress field due to autofrettage, whether ideal or realistic, tended to decrease the combined SIF $K_{IN} = K_{IP} - |K_{IA}|$. Therefore, to assess the fracture endurance and the fatigue life of a cylindrical, autofrettaged, pressure vessel containing such a network of cracks, it is necessary to determine the K_{IA}'s and the K_{IN}'s. This paper presents the K_{IA} and the K_{IN} distribution for numerous configurations of semi-circular and semi-elliptical, crack networks affected by pressure and autofrettage. The 3-D analysis is performed via the finite element (FE) method and the submodeling technique, employing singular elements along the crack front and the various symmetries of the problem. The networks considered included up to 128 equally spaced cracks in the radial direction; with relative, longitudinal crack spacing, $2c/d$, from 0.1 to 0.99; covered autofrettage level of 100 percent; employed a wide range of crack depth to wall thickness ratios, a/t, from 0.01 to 0.4; and, involved cracks with various ellipticities of crack depth to semi-crack length, a/c, from 0.2 to 2. The results clearly indicate that the combined SIFs are considerably influenced by the three-dimensionality of the problem and the Bauschinger effect to such an extent that cracks predicted closed by the ideal autofrettage model are predicted as remaining open by the realistic autofrettage model. In addition, the SIFs are found to depend upon the other parameters enumerated previously, namely: radial crack density, longitudinal crack spacing, crack depth, crack ellipticity, and the autofrettage level.

Keyword: Bauschinger Effect, Autofrettage, Combined SIF, crack networks

1 Introduction

Autofrettage was initially introduced to thick-walled cylinders, namely gun barrels, almost a century ago (Kendall (2000)) in order to increase their operational pressure. Further on, it was realized that the favorable compressive residual stresses introduced by autofrettage was additionally beneficial by impeding, or at least delaying, crack initiation and by slowing down fatigue crack growth thus extending the fatigue life of the cylinder. Such thick-walled cylinders may be exposed to high pressure cyclic loading, acute temperature gradients and a corrosive environment. As a result of these factors and the possible presence of stress concentrators such as gun rifling,

[1] Edward F. Cross School of Engineering, Walla Walla University, College Place, WA, 99115, USA
[2] Associate Dean, College of Engineering and Computing, and, Professor, Department of Mechanical and Materials Engineering, Florida International University, Miami, FL 33199, USA
[3] Aaron Fish Professor of Mechanical Engineering-Fracture Mechanics, Department of Mechanical Engineering and Pearlstone Center for Aeronautical Studies, Ben Gurion University of the Negev, Beer Sheva 84105 ISRAEL

numerous cracks develop at the inner surface of the cylinder. Experimental observations show that a large periodic array of almost identical semi-elliptical, radial and longitudinally-coplanar, internal cracks may develop at the inner surface of the cylinder. In order to predict the cylinder's loading capacity and its fatigue life span, the effective three dimensional stress intensity factors (SIF) – K_{Ieff} that exists at the crack front of these cracks must be evaluated. In general, K_{Ieff} results from three different loads: $\mathbf{K}_{IP}$ - the stress intensity factor caused by pressure; $\mathbf{K}_{IA}$ - the negative SIF due to the compressive residual stresses introduced by autofrettage, negative in the context of superposition; and $\mathbf{K}_{IT}$ - the SIF resulting from the temperature field. In the case of a typical gun barrel, K_{IT} values are found to be in general negative and much smaller in absolute terms than those of K_{IP} and K_{IA} (for example, Perl and Greenberg, (1999)). Therefore, the analysis of barrels usually neglects K_{IT} and is based on $\mathbf{K}_{IN}$ - the combined SIF, $K_{IN} = K_{IP} - |K_{IA}|$.

The effectiveness of autofrettage in reducing the combined SIF, K_{IN}, is directly proportional to the magnitude of the residual compressive stresses from the cylinder's inner wall and throughout the inner portion of the cylinder wall. For any given geometry of the cylinder and overstressing process, the level of the residual compressive stresses and their distribution is highly dependent on the specific characteristics of the cylinder material. As both hydraulic autofrettage and swage autofrettage involve loading and unloading of the cylinder during the process, the level of benefit that the resulting residual stress field can provide is highly influenced by the amount of Bauschinger Effect that the material exhibits.

Bauschinger (1881) discovered the effect bearing his name, and found that cyclic change in loading conditions resulting in plastic deformation causes continuous change of the yield stress. A material subjected to a certain amount of plastic deformation in tension (or compression) subsequently undergoing reversed loading i.e., compression (tension), often exhibits a reduction in its yield stress. The ratio between the reduced yield stress and the initial one is usually termed the *Bauschinger Ef-*

fect Factor (BEF). Therefore, the Bauschinger Effect (BE) might impact the residual stress field introduced by autofrettage as the process involves a loading-unloading cycle with plastic deformation. Milligan, Koo and Davidson (1966) studied experimentally the BE in a modified 4330 high-strength steel used for gun barrels in the mid 1960's. Their major conclusion was that the BE increases with increasing permanent strain up to about 2%. Thereafter, it tends to level off at a value of 0.35.

Others have attempted to incorporate the BE into autofrettage analysis, Chen (1986), Chaaban, Leung and Burns (1986), and Parker and Underwood (1998), among others. None of the models employed was able to simulate the complete nonlinearity of the unloading phase of autofrettage. In 1997, Jahed and Dubey suggested an improved algorithm that can account for the varying BEF within the re-yielding zone, which was further extended by Parker, Underwood and Kendall (1999). Its application by Parker and associates (1999, 2001) resulted in a more realistic evaluation of the autofrettage residual stress field.

Recently, the impact of the Bauschinger Effect on three-dimensional SIFs was investigated using the Parker (2001) data. One study evaluated the SIFs for internal radial cracks in a gun barrel with autofrettage (Perl, Levy and Rallabhandy (2006)) and another study explored internal longitudinally-coplanar cracks in a gun barrel (Levy, Perl and Kotagiri (2006)). Stress intensity factors due to autofrettage for a large number of crack configurations were evaluated. K_{IA} values were obtained with and without the Bauschinger Effect. In these studies, the Bauschinger Effect reduced the beneficial stress intensity factor due to autofrettage, K_{IA}, by up to 56%, as compared to the case of "ideal" autofrettage. Further, the Bauschinger Effect was found to reduce the combined stress intensity factor, K_{IN}, by 42-100% compared to their ideal autofrettage counterparts, in some cases.

The only attempt to address the problem of networks of radial and longitudinally-coplanar cracks in gun tubes was made about a decade ago by Perl, Levy and Wang (1997). That study inves-

tigated only pressure effects and found that K_{IP} decreased when the spacing for radial cracks decreased and increased when the spacing between longitudinal coplanar cracks decreased.

Since rifled gun barrels exhibiting such networks of radial and longitudinally coplanar cracks are typically autofrettaged, it is the intention of the present analysis to:

a. Determine the distributions of K_{IA}, the negative stress intensity factor due to autofrettage along the crack front of numerous crack networks of radial and longitudinally-coplanar, semi-elliptical crack configurations that may exist in a thick-walled cylinder with "realistic"- Bauschinger Effect Dependent Autofrettage (*BEDA*) based on Parker's (2001) model and to compare the results with K_{IA} values for "ideal"-Bauschinger Effect Independent Autofrettage (*BEIA*), based on Hill's (1950) solution.

b. Determine the distributions of the combined SIF, K_{IN}, along the crack front of numerous crack networks of radial and longitudinally-coplanar, semi-elliptical crack configurations that may exist in a thick-walled cylinder with "realistic" *BEDA* and to compare the results with K_{IN} values for "ideal" *BEIA*.

c. Extract the dependence of the favorable effect of autofrettage on the internal pressure in the barrel, p, and the cylinder's material yield stress, σ_{yp}, for both *BEDA* and *BEIA*,

d. Determine the impact of the BE on the total fatigue life of the thick-walled cylinder.

Though the numerical method used herein is the same as used in previous papers of two of the authors, the results obtained are new, very important and of practical use. Further, the use of realistic autofrettage is new for this problem.

2 Methodology

2.1 Simulation Of Autofrettage

The "ideal" plane-strain solution for a fully or partially autofrettaged thick-walled cylinder was derived by Hill (1950), assuming an elastic-perfectly-plastic material, using von Mises yield criterion and the incompressibility condition. The analysis yielded analytical expressions for the residual field stress components given by:

$$\sigma_{\text{rr}} = \begin{cases} \frac{\sigma_{yp}}{\sqrt{3}} \left[\left(2\ln\frac{r}{\rho} - 1 + \frac{\rho^2}{R_0^2} \right) - P_1 \left(\frac{1}{R_0^2} - \frac{1}{r^2} \right) \right]; \\ \qquad\qquad R_i \leq r \leq \rho \\ \frac{\sigma_{yp}}{\sqrt{3}} \left(\rho^2 - P_1 \right) \left(\frac{1}{R_0^2} - \frac{1}{r^2} \right); \\ \qquad\qquad \rho \leq r \leq R_0 \end{cases}$$

(1)

$$\sigma_{\theta\theta} = \begin{cases} \frac{\sigma_{yp}}{\sqrt{3}} \left[\left(2\ln\frac{r}{\rho} + 1 + \frac{\rho^2}{R_0^2} \right) - P_1 \left(\frac{1}{R_0^2} + \frac{1}{r^2} \right) \right]; \\ \qquad\qquad R_i \leq r \leq \rho \\ \frac{\sigma_{yp}}{\sqrt{3}} \left(\rho^2 - P_1 \right) \left(\frac{1}{R_0^2} + \frac{1}{r^2} \right); \\ \qquad\qquad \rho \leq r \leq R_0 \end{cases}$$

(2)

where r and θ are the radial and angular coordinates, σ_{yp} is the yield stress of the material, ρ is the radius of the autofrettage interface, and P_1 is given by the expression:

$$P_1 = \frac{R_i^2 \cdot R_o^2}{R_0^2 - R_i^2} \left[1 - \frac{\rho^2}{R_0^2} + 2\ln\frac{\rho}{R_i} \right]$$

(3)

The "realistic" autofrettage used in this investigation was evaluated numerically by Parker (2001) extending Jahed and Dubey's (1997) procedure. Parker (2001) incorporated the Bauschinger Effect in the unloading phase with variable BEF based on Milligan, Koo and Davidson (1966), assumed Engineering Plane Strain (open-end) conditions and used the von Mises yield criterion. Typical residual hoop stresses for various levels of "realistic" autofrettage (ε=10%-100%) for a cylinder of radii ratio of R_o/R_i=2 are given in Figure 8 of Parker, Underwood and Kendall (1999). An extensive comparison between the *BEDA* and *BEIA* autofrettage residual stress fields is given in Perl, Levy and Rallabhandy (2006).

The residual stress field pattern changes when cracking occurs at the inner surface of the cylinder. The evaluation of the redistribution of the

residual stresses in this instance is not straightforward. A proper active thermal load can be used to create thermal stresses, identical to the autofrettage stress field, in the cylinder as well as to accurately reproduce the stress redistribution resulting from the development of cracks or notches in the cylinder (Pu and Hussain (1983)). Hence, such an equivalent thermal load was implemented in the Finite Element (FE) analysis used in this investigation.

The equivalent thermal load for Hill's (1950) autofrettage case was derived analytically by Parker and Farrow (1980), and is given by the following temperature field:

$$T(r) = \begin{cases} T_i - \frac{T_i - T_\rho}{\ln \rho/R_i} \ln \frac{r}{R_i}; & R_i \le r \le \rho \\ T_\rho; & \rho \le r \le R_0 \end{cases} \quad (4)$$

where T_i is an arbitrary reference temperature usually chosen as nil, and the temperature gradient is given by:

$$T_i - T_\rho = \frac{2\sigma_{yp}}{\sqrt{3}} \cdot \frac{2(1-\upsilon) \ln \rho/R_i}{E\alpha} \quad (5)$$

where α is the linear coefficient of thermal expansion, E is the Young's modulus of elasticity and ν is the Poisson's ratio.

Parker's (2001) Bauschinger Effect Dependent Autofrettage (*BEDA*) field is given numerically in terms of the residual hoop stress values at discrete points throughout the cylinder's wall (see Fig. 8 in Parker (2001)). Perl (1988) provided an exact numerical algorithm that enables the direct evaluation of the equivalent temperature field for simulating any analytically or numerically expressed autofrettage residual stress field. In order to apply Perl's algorithm to Parker's *BEDA*, one needs to first evaluate the residual radial stress component, σ_{rr}, for Parker's solution,. This can be numerically extracted from equilibrium considerations. Once both $\sigma_{\theta\theta}^{BEDA}$ and σ_{rr}^{BEDA} are determined, the equivalent thermal load can be evaluated.

2.2 The Three-Dimensional Analysis

The three dimensional analysis is performed on an infinitely long, elastic cylinder of inner radius, R_i, outer radius, R_o, wall thickness, t, $(R_o/R_i = 2,$

$t = R_i)$. A segment of the cylinder showing six of the cracks is presented in Fig. 1a. The cylinder contains a network of cracks made up of an infinite array of identical semi-elliptical cracks of length, $2c$, and depth a (see Fig. 1a inset), located on n equi-angular ($\theta = 2\pi/n$) radial planes, each plane containing an infinite number of equally spaced longitudinal-coplanar cracks. The longitudinal distance between two adjacent crack centerlines is d. A Poisson ratio, ν, equal to 0.3, representing a steel cylinder is assumed in the analysis.

2.3 Finite Element Idealization

Due to the various symmetries of the geometrical configuration, only part of the cylinder must be analyzed. The planes of symmetry, $Z = 0$, $Z = d/2$, $\theta = 0°$, $\theta = \pi/n°$ (see Fig. 1b) allow us to model only that part of the cylinder enclosed within them. The cylinder is assumed to freely move in the axial direction as is commonly hypothesized, meaning it is free of loads and unconstrained at its ends. As previously described, the autofrettage residual stress field for both *BEDA* and *BEIA* is simulated by the proper equivalent thermal load.

The model is solved using ANSYS, a standard FE code, in two consecutive steps via the submodeling technique. In the first step, a global mesh of the entire segment is generated using 10-node tetrahedron elements while applying a half automatic meshing procedure. The elements are varied in size, small near the crack front and gradually increased when moving away from it. The displacements obtained from the global mesh are used as boundary conditions for the submodel in the second stage.

In the second step, a toroidal submodel is created covering the crack front area with three layers of 20-node isoparametric elements (see Fig. 2). Elements collapsed to wedges form the singular elements at the crack front (Barsoum (1976); Akamatsu, Nakane and Ohno (2005)) for the first layer as well as two additional element layers above the first layer. The displacements from the global solution act as boundary conditions to the outer surface of the third layer. A comparison between the stress fields on the interface surface of
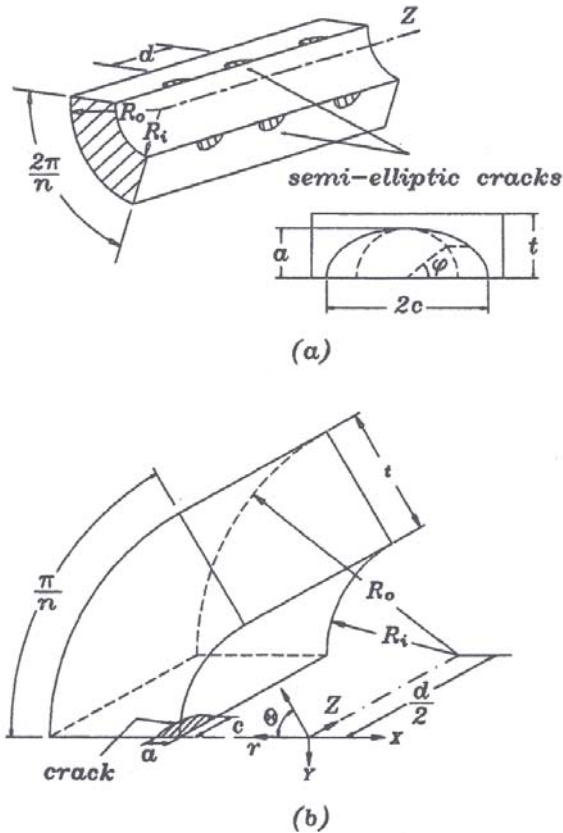
Figure 1: (a) Segment of crack network considered for the model employing planes of symmetry Z=0, $\theta = 0$, $\theta = 2\pi/n$. Inset provides the definition of the angle φ for the SIF evaluation (b) Cylinder segment employed in the FE model
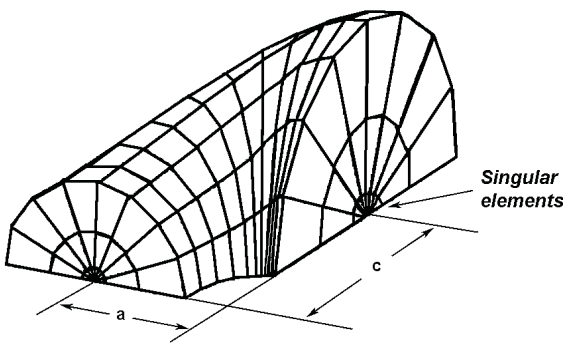

Figure 2: The meshed submodel

the global and the submodels is performed to ensure a smooth transition between the two stages.

Convergence tests were performed using the stress intensity factor as the convergence crite-

rion. Based on these trials, it is anticipated that the level of error will be less than 3% for meshes of more than 100,000 degrees of freedom (DOF). Hence, in order to maintain good accuracy while using reasonable computer resources, most meshes contained about 100 thousand DOF; high n and/or $2c/d$ required 5-10 million DOF. The software automatically adjusted elements shape and aspect ratio for all meshes.

SIFs are calculated from the submodel results using the code's crack-face displacement extrapolation procedure. The SIFs were calculated every 9 degrees from $\phi = 0°$ to $90°$ (see Fig. 1a). The results of the present model were validated against K_{IN}, K_{IP}, and K_{IA} values obtained by Perl and Nachum (2000, 2001) for "ideal" autofrettage, and against K_{IA} values obtained by Perl, Levy and Rallabhandy (2006) and Levy, Perl and Kotagiri (2006) for "realistic" autofrettage. All the results were found to be in excellent agreement.

3 Results And Discussion

To study the impact of the Bauschinger Effect, as well as that of the different geometrical parameters on the combined stress intensity factor, K_{IN}, solutions for a large number of crack configurations are obtained. In order to maintain the same accuracy for K_{IP}, and K_{IA}, and thus for K_{IN}, K_{IP} and K_{IA} for each crack configuration are evaluated using the identical finite element breakdowns.

SIF distributions for radial semi-elliptical or semi-circular crack arrays are solved for the following set of parameters: $n =$1, 2,4, 8, 16, 32, 64 and 128 cracks; with longitudinal crack spacing $2c/d$=0.1, 0.25, 0.5, 0.75, 0.94 and 0.99; crack ellipticities a/c = 0.2, 0.5, 1, 1.5 and 2; ratio of crack depth to wall thickness $a/t =$0.01, 0.03, 0.05, 0.1, 0.15, 0.2 and 0.4 common in cylinders with autofrettage levels of $\varepsilon = 100\%$. Typical results will be presented, and, for the sake of clarity and usefulness, not all cases will be displayed.

Normalized K_{IA} results for *BEDA* and *BEIA* are compared to those of Perl, Levy and Rallabhandy (2006), labeled Vamshi, and Perl and Nachum (2000), labeled Assaf, respectively, as the radial cracks only case is akin to the $2c/d = 0$ case.

They are normalized to allow for comparison and to allow for combination with those SIF values of K_{IP}, in order to obtain K_{IN}. The normalizing factor is:

$$K_0 = \frac{pR_i}{t}\sqrt{\frac{\pi a}{Q}} \qquad (6)$$

where pR_i/t represents the average circumferential stress in the cylinder, and Q is the shape factor for an elliptical crack. Q, which represents the square of a complete elliptic integral of the second kind, is usually approximated by:

$$\begin{aligned} Q &= 1 + 1.464\left(\frac{a}{c}\right)^{1.65} \quad \text{for } a/c \leq 1 \\ Q &= 1 + 1.464\left(\frac{c}{a}\right)^{1.65} \quad \text{for } a/c \geq 1 \end{aligned} \qquad (7)$$

In the present analysis σ_{yp} is chosen to be 1172 MPa (170 ksi), representing the yield stress of a typical gun barrel steel. The operating pressure, p, will be taken as 330 MPa, for classic gun barrels. For modern gun barrels where the operating pressure is 607 MPa, one has only to multiply the K_{IA} results provided by 1.93/3.55 and add to the K_{IP} results to obtain the relevant K_{IN} SIF values. Typical results are presented separately for a fully autofrettaged, thick-walled cylinders. In the following graphs, results for *BEIA* will be presented with solid symbols and/or solid lines, whereas *BEDA* results will be presented by clear symbols and/or dashed lines.

3.1 Autofrettage Results

3.1.1 Network of Semi-Circular Cracks, a/c=1

The autofrettage results will be presented first for networks of radial and longitudinally-coplanar cracks as such results have not been discussed elsewhere. As such, we provide typical results found. In Fig. 3 the data for a network of shallow, semi-circular cracks, $a/c = 1$, $a/t = .05$, $n = 2$ and for various values of $2c/d = 0.1$ to 0.94 is presented. Note that both the *BEIA* and *BEDA* for all $2c/d$ values follow an ordered pattern where the maximum is at $\phi=0$ deg, i.e., where the crack surface meets the inner wall of the cylinder bore, and that the magnitude of the SIFs decrease as ϕ increases. We note that *BEIA* values are larger

than *BEDA* values and that as $2c/d$ increases, the normalized K_{IA} values also increase. This behavior is identical to the K_{IA} behavior found in the investigation of longitudinally-coplanar cracks only (Levy, Perl and Kotagiri (2006)). Note that because the K_{IA} values are higher than the $n = 1$ comparison results, irrespective of type of autofrettage, the $n = 2$ case shown here follows the trends found in the study of the radial cracks (Perl, Levy and Rallabhandy (2006)). When compared to the $n = 2$, $2c/d = 0$ case, the normalized K_{IA} values can be over 108% higher for *BEIA* and about 100% higher for *BEDA* for $2c/d = 0.94$.
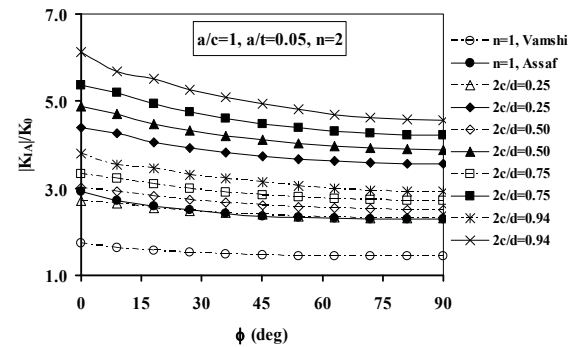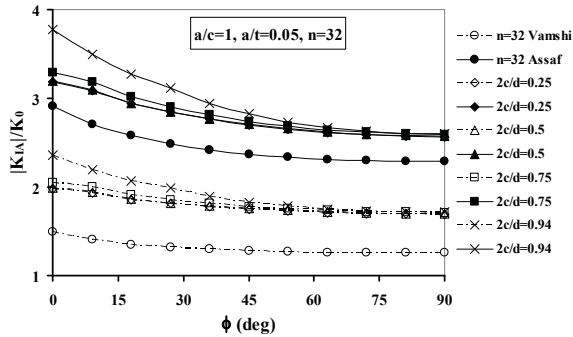

Figure 3: Normalized Autofrettage SIF for a network of shallow, semi-circular cracks $a/c = 1$, $a/t = 0.05$, $n = 2$ and various $2c/d$ for *BEIA* (dark/solid symbols) and *BEDA* (clear/dashed symbols)

Figure 4 provides the data for normalized autofrettage SIF for a network of shallow, semi-circular cracks, $a/c = 1$, $a/t = .05$, $n = 32$ and for various values of $2c/d = 0.1$ to 0.94. Again, we note that the maximums occur at $\phi=0$ deg and that the curves are monotonically decreasing as ϕ increases. In comparison to Fig. 3, the values of magnitude for the SIFs for both types of autofrettage in Fig. 4 are less than their counterparts, meaning that the trends with respect to radial cracks found in Perl, Levy and Rallabhandy (2006) are maintained. The trends with respect to the longitudinally-coplanar cracks also follow the same pattern of increasing in magnitude as $2c/d$ increases. When compared to the $n = 32$, $2c/d = 0$ case, the normalized K_{IA} values can be

over 14% higher for *BEIA* and about 36% higher for *BEDA* for $2c/d = 0.25$. For $2c/d = 0.94$, the values are at 29% and 57% higher, respectively, indicating that as n increases the differences decline.

Figure 4: Normalized Autofrettage SIF for a network of shallow, semi-circular cracks $a/c = 1$, $a/t = 0.05$, $n = 32$ and various $2c/d$ for *BEIA* (dark/solid symbols) and *BEDA* (clear/dashed symbols)

3.1.2 Networks of Slender, Semi-Elliptical Cracks, a/c<1

Figure 5 provides typical data for typical examples of normalized autofrettage SIF for a network of shallow, slender, semi-elliptical cracks, $a/c = 0.5$, $a/t = .05$, $n = 2$ and various values of $2c/d = 0.1$ to 0.94. We note the curves form a lazy "S", that the maximums always occur at ϕ=90 deg, where the cracks are their deepest in the wall thickness, and that the curves have a minimum at about ϕ=9 deg. We note that *BEIA* values are larger than *BEDA* values and that as $2c/d$ increases, the normalized K_{IA} values also increase. This behavior is identical to the K_{IA} behavior found in the investigation of longitudinally-coplanar cracks only (Levy, Perl and Kotagiri (2006)). Note that because the K_{IA} values are higher than the $n = 1$ comparison results, irrespective of type of autofrettage, the $n = 2$ graphs shown here follow the trends found in the radial cracks study (Perl, Levy and Rallabhandy (2006)). When compared to the $n = 2$, $2c/d = 0$ case, the normalized K_{IA} values can be

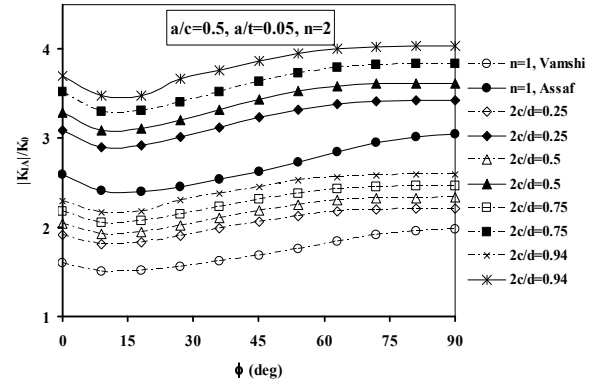over 31% higher for *BEIA* and 22% for *BEDA* for $2c/d = 0.94$.

Figure 5: Normalized Autofrettage SIF for a network of shallow, slender, semi-elliptical cracks $a/c = 0.5$, $a/t = 0.05$, $n = 2$ and various $2c/d$ for *BEIA* (dark/solid symbols) and *BEDA* (clear/dashed symbols)
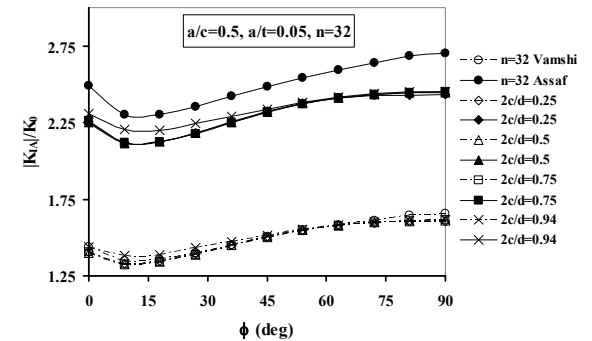

Figure 6: Normalized Autofrettage SIF for a network of shallow, slender, semi-elliptical cracks $a/c = 0.5$, $a/t = 0.05$, $n = 32$ and various $2c/d$ for *BEIA* (dark/solid symbols) and *BEDA* (clear/dashed symbols)

Figure 6 provides the data for normalized autofrettage SIF for a network of shallow, slender, semi-elliptical cracks, $a/c = 0.5$, $a/t = .05$, $n = 32$ and for various values of $2c/d = 0.1$ to 0.94. Again, we note the curves form a lazy "S", that the maximums occur at ϕ=90 deg, where the cracks are their deepest in the wall thickness, and that the curves have a minimum at about ϕ=9 deg. In contrast to Fig. 5, the values of

magnitude for the SIFs for both types of autofrettage in Fig. 6 are less than their counterparts, meaning that the trends with respect to radial cracks found in Perl, Levy and Rallabhandy (2006) are maintained. The trends with respect to the longitudinally-coplanar cracks follow those found in Levy, Perl and Kotagiri (2006), namely, that the values increase as $2c/d$ increases. When compared to the $n = 32$, $2c/d = 0$ case, the normalized K_{IA} values can be over 9% lower for *BEIA* and 3% lower for *BEDA* for $2c/d = 0.94$.

3.1.3 Networks of Transverse, Semi-Elliptical Cracks, a/c>1

Figure 7 provides typical data for normalized autofrettage SIF for a network of shallow, transverse, semi-elliptical cracks, $a/c = 1.5$, $a/t = .05$, $n = 4$ and for various values of $2c/d = 0.1$ to 0.99. Again, we note the behavior of the curves are similar to the semi-circular $a/c = 1$ case. The SIF maximums occur at $\phi=0$ deg, where the cracks intersect the bore of the cylinder and continue to decrease to $\phi=90$ deg. We note that *BEIA* values are larger than *BEDA* values and that as $2c/d$ increases, the normalized K_{IA} values also increase. This behavior is identical to the K_{IA} behavior found in the investigation of longitudinally-coplanar cracks only (Levy, Perl and Kotagiri (2006)). When compared to the $n = 4$, $2c/d = 0$ case, the normalized K_{IA} values can be over 88% higher for *BEIA* and about 98% higher for *BEDA* for $2c/d = 0.99$.

Figure 8 provides typical data for normalized autofrettage SIF for a network of shallow, transverse semi-elliptical cracks, $a/c = 1.5, a/t = .05$, $n = 64$ and for various values of $2c/d = 0.1$ to 0.99. Again, we note that the maximums occur at $\phi=0$ deg and that the curves are monotonically decreasing as ϕ increases. In comparison to Fig. 7, the values of magnitude for the SIFs for both types of autofrettage in Fig. 8 are less than their counterparts, meaning that the trends with respect to radial cracks found in Perl, Levy and Rallabhandy (2006) are maintained. The trends with respect to the longitudinally-coplanar cracks follow those found in Levy, Perl and Kotagiri (2006). When compared to the $n = 64$, $2c/d = 0$ case, the nor-
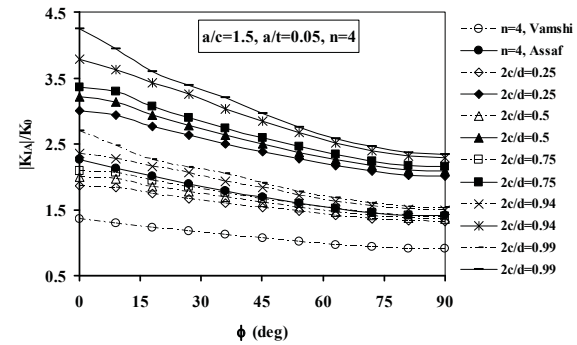

Figure 7: Normalized Autofrettage SIF for a network of shallow, transverse, semi-elliptical cracks $a/c = 1.5$, $a/t = 0.05$, $n = 4$ and various $2c/d$ for *BEIA* (dark/solid symbols) and *BEDA* (clear/dashed symbols)
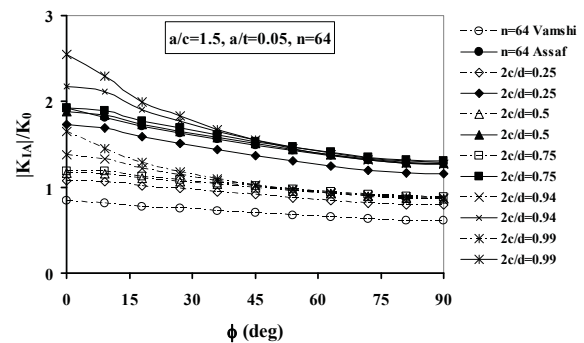

Figure 8: Normalized Autofrettage SIF for a network of shallow, transverse, semi-elliptical cracks $a/c = 1.5$, $a/t = 0.05$, $n = 64$ and various $2c/d$ for *BEIA* (dark/solid symbols) and *BEDA* (clear/dashed symbols)

malized K_{IA} values can be 13% higher for *BEIA* and about 62% higher for *BEDA* for $2c/d = 0.94$. Again, we note the decrease in these values as n increases.

3.1.4 Effect of Dimensionless Crack Length, a/t, on Autofrettage Stress Intensity Factors

Figures 9a, b and c provide typical data for networks of shallow ($a/t = 0.05$) and deeper ($a/t = 0.2$) slender, semi-elliptical cracks for $a/c=0.5$, $n=8$ and various values of $2c/d$. It would appear that the K_{IA} values would decrease as a/t increases. But this is an artifact of the normalizing

factor K_0 that contains the $\sqrt{a}$ and is in the denominator. Since the deeper crack has a larger a, then K_0 is larger making the normalized value of K_{IA} appear smaller. This artifact would also exist when comparing networks of shallow and deeper, semi-circular cracks and networks of shallow and deeper, transverse, semi-elliptical cracks, with all other parameters being unchanged (a/c, n, autofrettage level). However, what is not an artifact is that the *BEIA* values and the *BEDA* values are becoming closer. This is because for cracks in this range of a/t, the residual stress fields of both the *BEIA* and *BEDA* are very similar to each other (see Perl, Levy and Rallabhandy (2006) discussion of residual stress field). When compared to their respective *n=8, 2c/d=0* case at $a/t = 0.05$, the normalized K_{IA} values are within 2% for *BEIA* and *BEDA* for all $2c/d$. However, for the deeper crack, $a/t = 0.2$, the normalized K_{IA} values are within 10% of their respective *n=8, 2c/d=0* case for *BEIA* and *BEDA* for all $2c/d$ cases except $2c/d = 0.99$ case. When one looks at the much deeper crack, $a/t = 0.4$, and uses the $2c/d = 0.1$ case for comparison, then the normalized K_{IA} values are within 2% for all the *BEIA* and *BEDA* cases except $2c/d = 0.99$, where they are within 14%.

3.2   Combined Stress Intensity Factor Results

The combined stress intensity factor, K_{IN}, results are presented next for networks of radial and longitudinally-coplanar cracks. As such, we provide typical results found. In all the graphs shown, autofrettage, whether *BEDA* or *BEIA*, reduces the combined SIF, K_{IN}. Normalized K_{IN} results for *BEDA* and *BEIA* are compared to those of Perl, Levy and Rallabhandy (2006), labeled Vamshi, and Perl and Nachum (2001), labeled Assaf, respectively, as the radial cracks only case is akin to the $2c/d = 0$ case. They are normalized to allow for comparison and to allow for combination with those SIF values of K_{IP}, in order to obtain K_{IN}. The normalizing factor is given by Eq. 6.
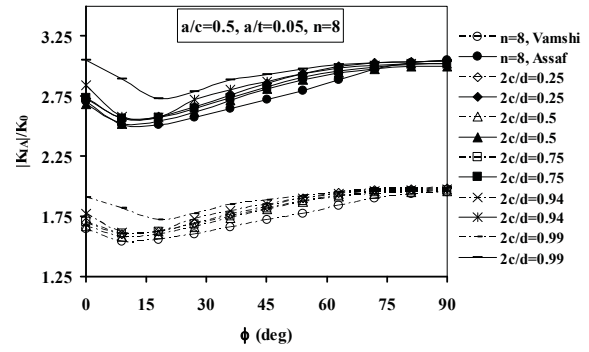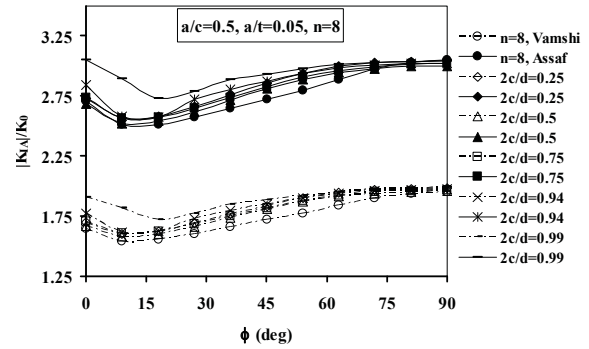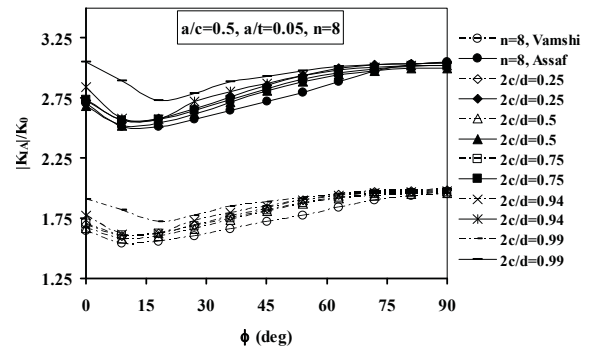

Figure 9a: Normalized Autofrettage SIF for a network of slender, semi-elliptical cracks $a/c = 0.5$, $a/t = 0.05$, $n = 8$ for various $2c/d$ for *BEIA* (dark/solid symbols) and *BEDA* (clear/dashed symbols)

Figure 9b: Normalized Autofrettage SIF for a network of slender, semi-elliptical cracks $a/c = 0.5$, $a/t = 0.2$, $n = 8$ for various $2c/d$ for *BEIA* (dark/solid symbols) and *BEDA* (clear/dashed symbols)

Figure 9c: Normalized Autofrettage SIF for a network of slender, semi-elliptical cracks $a/c = 0.5$, $a/t = 0.4$, $n = 8$ for various $2c/d$ for *BEIA* (dark/solid symbols) and *BEDA* (clear/dashed symbols)

3.2.1 Networks of Semi-Circular Cracks (a/c=1)

In Fig. 10 the data for a network of shallow, semi-circular cracks, $a/c = 1$, $a/t = .05$, $n = 2$ and for various values of $2c/d = 0.1$ to 0.99 are presented. Note that the *BEIA* sport maxima at $\phi=90$ deg for all $2c/d$ values and are closed for all cases except $n = 1$ (the K_{IN}/K_0 values are less than 0). Thus, the $n = 1$ case is the most critical case for the *BEIA*. We note that the cracks in all the *BEDA* cases are open and that a transition exists in the location of the maximum ($\phi=0$ deg for $2c/d$ values 0.25 or less and $\phi=90$ deg for $2c/d$ values greater than 0.25). Thus in the *BEDA* cases, the maximum also occurs at $2c/d = 0$. In all cases, the *BEDA* values are larger than their *BEIA* counterparts. These trends for $2c/d$ follow those found in Levy, Perl and Kotagiri (2006), yet the results are lower due to the number of radial cracks being 2. When compared to the $2c/d = 0, n = 2$ case K_{IN}/K_0 values, as $2c/d$ increases, the maximums decrease by up to 95% for the *BEDA* cases. This means that the results for the radial crack only situation can serve as upper bounds for calculating the life cycle for this type of network.
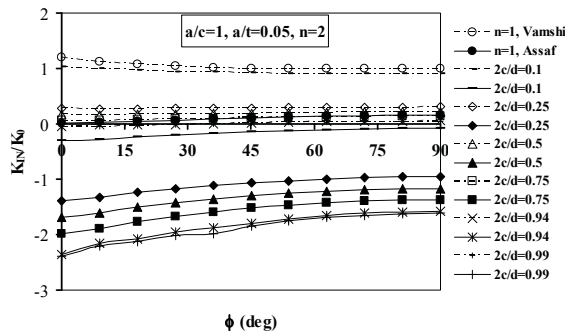

Figure 10: Normalized Combined SIF for a network of shallow, semi-circular cracks $a/c = 1$, $a/t = 0.05$, $n = 2$ and various $2c/d$ for *BEIA* (dark/solid symbols) and *BEDA* (clear/dashed symbols)

In Figs. 11 and 12 are presented typical results for a network of shallow, semi-circular cracks, $a/c = 1$, $a/t = .05$, $2c/d = 0.1$ and $2c/d = 0.75$, respectively, for various values of $n = 1 - 64$. In both cases, the results follow the trends given in
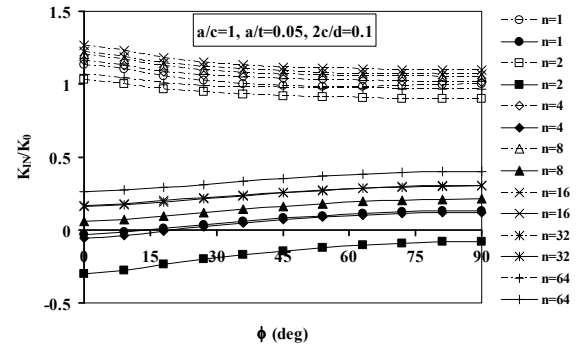

Figure 11: Normalized Combined SIF for a network of shallow, semi-circular cracks $a/c = 1$, $a/t = 0.05$, $2c/d = 0.1$ and various n for *BEIA* (dark/solid symbols) and *BEDA* (clear/dashed symbols)
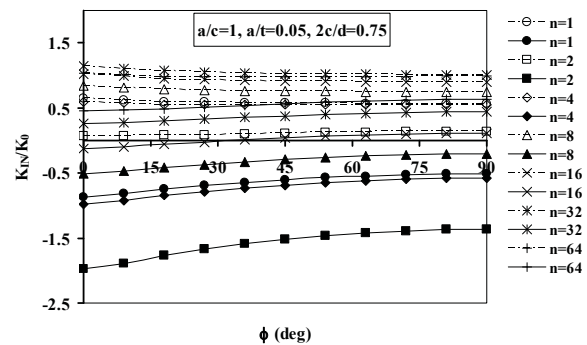

Figure 12: Normalized Combined SIF for a network of shallow, semi-circular cracks $a/c = 1$, $a/t = 0.05$, $2c/d = 0.75$ and various n for *BEIA* (dark/solid symbols) and *BEDA* (clear/dashed symbols)

Perl, Levy and Rallabhandy (2006) where their results can be thought of as $2c/d = 0$ case. We note that the *BEDA* values are larger than the *BEIA* counterparts and that the *BEIA* sport maxima at $\phi=90$ deg for all n values and can be open, partially closed or closed depending on n. The cracks under the influence of *BEDA* are open and have maxima at $\phi=0$ deg. We see that the most critical case is $n = 16$ for $2c/d = 0.1$ and $n = 32$ for $2c/d = 0.75$; for the *BEIA* cases, the largest K_{IN}/K_0 values occur for large n as well. We note that at $2c/d = 0.1$, the K_{IN}/K_0 curves for $n = 1 - 64$ are in a tighter group than those for $2c/d = 0.75$, e.g., the *BEDA* cases are within 11%

of each other.

3.2.2 Networks of Slender, Semi-Elliptical Cracks (a/c<1)

Figures 13, 14, 15 and 16 provide typical results obtained for the combined SIFs along the crack fronts of networks of slender, semi-elliptical cracks. Figure 13 provides the data for shallow, semi-elliptical cracks, $a/c = 0.5$, $a/t = .05$, $n = 2$ and for various values of $2c/d = 0.1$ to 0.94. Again, we note that the maxima occur at ϕ=90 deg for the *BEDA* cases, whereas the maxima for the *BEIA* cases occur somewhere between 9 and 18 deg. It is noted that the cracks studied in *BEDA* cases are completely open, while those of the *BEIA* cases are completely closed. This follows the trends found in Levy, Perl and Kotagiri (2006), equivalent to the $n = 1$ case. However, the trends here show that as $2c/d$ increases, the SIF values decrease, which seems to conflict with the trends found in Levy, Perl and Rallabhandy (2006). For the *BEDA* cases the maximum K_{IN}/K_0 values fall up to 46% below the $n = 2$, *Vamshi* results, while for the *BEIA* cases the maximum K_{IN}/K_0 values fall up to 146% below the *n=2, Assaf* results.

Figure 14 provides the normalized combined SIF data for shallow, slender, semi-elliptical cracks, $a/c = 0.5$, $a/t = .05$, $2c/d = 0.1$ and for various values of $n = 1 - 64$. The maxima for the *BEDA* and the *BEIA* cases occur at 90 deg; however, the character of the curves depends upon the type of autofrettage. There appears to be a local maximum for the *BEIA* curves between 9 and 18 deg, but an absolute maximum at ϕ=90 deg. Again the SIF values along the crack front for *BEDA* are larger than those of *BEIA*, and the most critical cases occur when $n > 1$, here $n = 16$ for *BEIA* and $n = 32$ for *BEDA*. Also, it is seen that the *BEDA* data increases then decreases as n increases, and, the *BEIA* data increases as n increases. *BEDA* cracks are open, while *BEIA* cracks are closed. All these results follow the trends reported in Perl, Levy and Rallabhandy (2006), except for the local maximum found in the *BEIA* curves. This, however, **is** a phenomenon seen in the Levy, Perl and Kotagiri (2006) data for longitudinal-coplanar cracks. Lastly, the maxima of the *BEDA* and *BEIA*

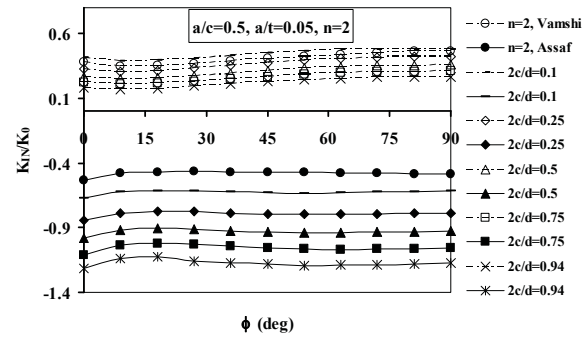data are all within 16% and 41% of each other, respectively.

Figure 13: Normalized Combined SIF for a network of shallow, slender, semi-elliptical cracks $a/c = 0.5$, $a/t = 0.05$, $n = 2$ and various $2c/d$ for *BEIA* (dark/solid symbols) and *BEDA* (clear/dashed symbols)
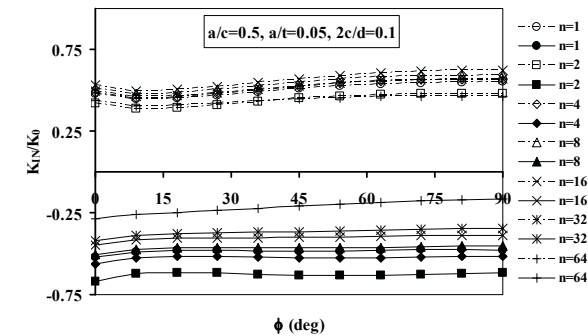

Figure 14: Normalized Combined SIF for a network of shallow, slender, semi-elliptical cracks $a/c = 0.5$, $a/t = 0.05$, $2c/d = 0.1$ and various n for *BEIA* (dark/solid symbols) and *BEDA* (clear/dashed symbols)

Figure 15 provides the normalized combined SIF data for shallow, slender, semi-elliptical cracks, $a/c = 0.5$, $a/t = .05$, $2c/d = 0.75$ and for various values of $n = 1 - 64$. The trends are similar to Fig. 14; however, the SIF values are larger, there is a larger spread in the data between the different curves, and the $n = 32$ and $n = 64$ set of the *BEIA* cracks are partially open. The maxima of the *BEDA* and *BEIA* data are all within 45% and 104% of each other, respectively.
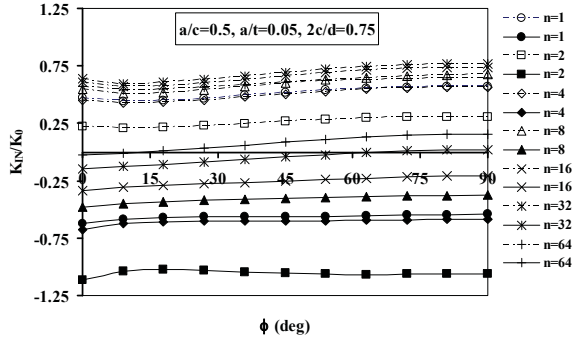
Figure 15: Normalized Combined SIF for a network of shallow, slender, semi-elliptical cracks $a/c = 0.5$, $a/t = 0.05$, $2c/d = 0.75$ and various n for *BEIA* (dark/solid symbols) and *BEDA* (clear/dashed symbols)

Figure 17: Normalized Combined SIF for a network of deeper, slender, semi-elliptical cracks $a/c = 0.5$, $a/t = 0.4$, $n = 8$ and various $2c/d$ for *BEIA* (dark/solid symbols) and *BEDA* (clear/dashed symbols)
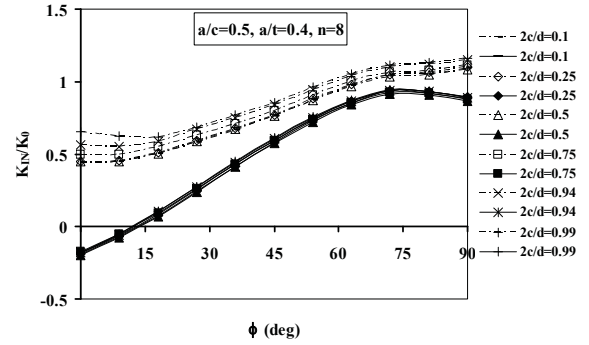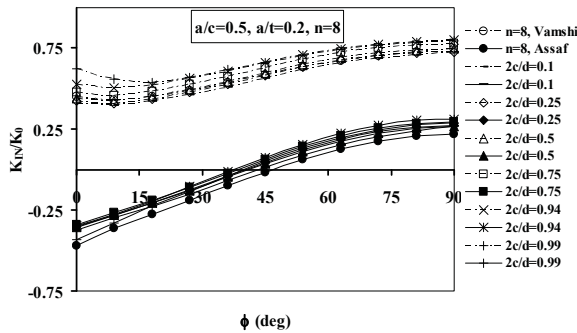

Figure 16: Normalized Combined SIF for a network of deeper, slender, semi-elliptical cracks $a/c = 0.5$, $a/t = 0.2$, $n = 8$ and various $2c/d$ for *BEIA* (dark/solid symbols) and *BEDA* (clear/dashed symbols)

Figure 16 provides typical normalized combined SIF data for a network of deeper, slender, semi-elliptical cracks ($a/c = 0.5$, $a/t = 0.2$, $n = 8$). We note that deeper cracks produce higher values of K_{IN}/K_0. Also, as $2c/d$ increases, the normalized SIF values also increase. Deeper cracks have their maxima at ϕ=90 deg, and, for all the $2c/d$ cases presented, the network of *BEDA* cracks are open and while those for *BEIA* can be partially open (here ϕ from 0 deg to 36-45 deg). The maxima of the *BEDA* and *BEIA* data are all within 8% and 41% of each other, respectively. The results shown follow the trends of Perl, Levy and Rallabhandy (2006) and Levy, Perl and Kotagiri (2006).

Figure 17 provides the data for even deeper, slender, semi-elliptical cracks ($a/c = 0.5$, $a/t = 0.4$, $n = 8$), almost half-way through the cylinder wall. We note that deeper cracks produce higher values of K_{IN}/K_0 and larger differences between maxima and minima. Also, as $2c/d$ increases, the normalized SIF values also increase. Deeper cracks have their maxima at ϕ=90 deg (*BEDA*) or near the deepest point (*BEIA*), and, for all the $2c/d$ cases presented, the network of *BEDA* cracks are open and those for *BEIA* are partially open. We note that the section of the crack that is closed is becoming smaller (here ϕ from 0 deg to 12 deg). The groups of curves are also becoming tightly bunched. The maxima of the *BEDA* and *BEIA* data are all within 3.5% and 4% of each other, respectively. The artifact described in Section 3.1.4 is also seen here. The actual K_{IN} values for $a/t = 0.4$ are higher than those for $a/t = 0.2$. What has been described for Fig. 17 also occurs for deeper, semi-circular cracks ($a/c = 1$), and also for deeper, transverse, semi-elliptical cracks ($a/c = 1.5$).

3.2.3 Networks of Transverse, Semi-Elliptical Cracks (a/c>1)

Figures 18 and 19 provide typical results obtained for the combined SIFs along the crack fronts of networks of transverse, semi-elliptical cracks. Figure 18 provides the data for shallow, semi-

elliptical cracks, $a/c = 1.5$, $a/t = .05$, $n = 4$ and for various values of $2c/d = 0.1$ to 0.99. Note that the *BEIA* show maxima at ϕ=90 deg for all $2c/d$ values and are closed for $2c/d > 0.1$. Thus, the $2c/d = 0$ case is the most critical case for the *BEIA*. In the *BEDA* cases, the maximum exists at ϕ=0 deg. In the *BEIA* cases K_{IN} values decrease with increasing $2c/d$. These trends for $2c/d$ follow those found in Levy, Perl and Kotagiri (2006). In the *BEDA* cases, the K_{IN} decreases then increase as $2c/d$ increases.
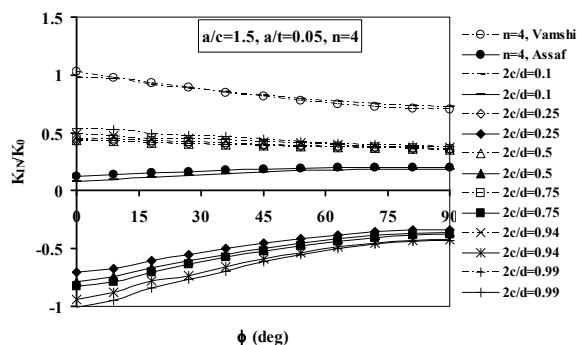

Figure 18: Normalized Combined SIF for a network of shallow, transverse, semi-elliptical cracks $a/c = 1.5$, $a/t = 0.05$, $n = 4$ and various $2c/d$ for *BEIA* (dark/solid symbols) and *BEDA* (clear/dashed symbols)
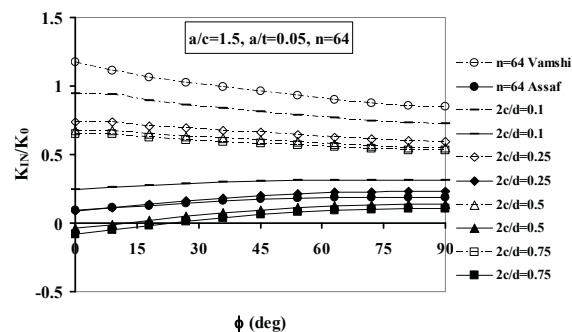

Figure 19: Normalized Combined SIF for a network of shallow, transverse, semi-elliptical cracks $a/c = 1.5$, $a/t = 0.05$, $n = 64$ and various $2c/d$ for *BEIA* (dark/solid symbols) and *BEDA* (clear/dashed symbols)

Figure 19 provides typical data for normalized combined SIF for a network of shallow, trans-

verse semi-elliptical cracks, $a/c = 1.5$, $a/t = .05$, $n = 64$ for various values of $2c/d = 0.1$ to 0.75. The $2c/d$ curves for 0.94 and 0.99 are not very different from the $2c/d = 0.75$ curves and are not included. Again, we note that the maximums occur at ϕ=0 deg for the *BEDA* data and at 90 deg for the *BEIA* data. In comparison to Fig. 18, the values of magnitude for the combined SIFs for both types of autofrettage have increased, meaning that the trends with respect to radial cracks found in Perl, Levy and Rallabhandy (2006) are maintained. The $a/c = 1.5$ trends follow those found for $a/c = 1$ (Fig. 10) for the *BEDA* data, namely that as $2c/d$ increases, the K_{IN} values decrease. However, the trends in K_{IN} change for the *BEIA* data as $2c/d$ increases; first they increase, then they decrease as in Fig. 18. Also, because the K_{IN} values are higher, the *BEIA* trends indicate that even at 64 cracks, the cracks are partially closed.

4 Conclusions

This paper presents the K_{IA} and the K_{IN} distribution for numerous configurations of semi-circular and semi-elliptical, crack networks affected by pressure and autofrettage. Though other elegant methods to solve crack problems exist (see, for example, So, Lau and Ng (2004)), we employed what was available, namely the ANSYS FE code. The crack networks considered included up to 128 equally spaced cracks in the radial direction; with relative, longitudinal crack spacing, $2c/d$, from 0.1 to 0.99; autofrettage level of 100 percent; employed a wide range of crack depth to wall thickness ratios, a/t, from 0.01 to 0.4; and, involved cracks with various ellipticities of crack depth to semi-crack length, a/c, from 0.2 to 2. The results clearly indicate that the combined SIFs are influenced considerably by the three-dimensionality of the problem and the Bauschinger effect to such an extent that cracks predicted closed or partially closed by the ideal autofrettage model (*BEIA*) are predicted as remaining open by the realistic autofrettage model (*BEDA*). The magnitude of the maximal combined SIF, $K_{Nmax,}$ is determined by the cylinder's material susceptibility to the Bauschinger Effect

and by the yield stress-to-pressure ratio as explained in Perl, Levy and Rallabhandy (2006). As an example of the impact BE might have on the fatigue life of the cylinder assumed here, the ratio between $K_{Nmax}(BEDA)/K_{Nmax}(BEIA)$ can vary in the $n = 32$ case, for example, between 1.34 (for $a/t = 0.2$, $a/c = 1.5$, and $2c/d = 0.75$) to 4.4 (for $a/t = 0.05$, $a/c = 1.0$, and $2c/d = 0.99$). As a first crude approximation, if a Paris exponent of n_P=3.0 is assumed, typical of thick-walled cylinder material used in gun barrels, the ratio of the fatigue lives would be $N_f(BEDA)/N_f(BEIA) =$ 0.01-0.42, namely, the BE might reduce the total fatigue life by a factor of about 2 to 100. In certain cases, when autofrettage completely dominates the pressure, a theoretically infinite fatigue life is predicted for *BEIA* versus a finite fatigue life for *BEDA*. For larger values of yield stress-to-pressure ratios, as in the case of modern pressure vessels, this factor can be much smaller. In addition, the SIFs are found to depend upon the other parameters enumerated previously, namely: radial crack density, longitudinal crack spacing, crack depth, crack ellipticity, and the autofrettage level. For small cracks the results between *BEDA* and *BEIA* autofrettage are quite different; yet, as crack depth increases the differences decrease. This is an outcome of the fact that realistic autofrettage affects stress fields closer to the cylinder bore and less so as one goes deeper into the cylinder wall (see Parker (2001)). One notes that in the preceding example the ratio between $K_{Nmax}(BEDA)/K_{Nmax}(BEIA)$ for $a/t = 0.2$ is 30% of the value of the ratio for $a/t = 0.05$ as corroborating support.

Based on the data we have shown in this paper, it is conjectured that the dominant effect is that of the radial cracks and that as the cracks come closer to each other, their effect of decreasing the magnitude of K_{IA} dominates the effect caused by the convergence of cracks in the longitudinal-coplanar direction, thereby modifying the order of the curves for the longitudinal crack spacing, $2c/d$.

References

Akamatsu, M.; Nakane, K.; Ohno N. (2005): A Virtual Crack Closure-Integral Method (VCCM) for Three-Dimensional Crack Problems Using Linear Tetrahedral Finite Elements. *CMES: Computer Modeling in Engineering & Sciences,* vol. 10, pp. 229-238.

Barsoum, R. S. (1976): On the use of isoparametric finite elements in linear fracture mechanics. *Int. J. Num. Meth. in Eng.*, vol. 10, pp. 25-37.

Bauschinger, J. (1881): Uber die veranderung der elasticitätsgrenze und des elasticitätsmoduls verschiedener metalle. *Zivilingenieur*, vol. 27, columns 289-348.

Chaaban, A.; Leung, K.; Burns, D. J. (1986): Residual stresses in autofrettaged thick-walled high pressure vessels. *ASME PVP* vol. 110, pp. 55-60.

Chen, P. C. T. (1986): Bauschinger and hardening effects on residual stresses in autofrettaged thick-walled cylinders. *Trans. ASME, J. Pressure Vessel Tech.*, vol. 108, pp. 108-112.

Hill, R. (1950): *The mathematical theory of plasticity*, Clarendon Press, Oxford.

Jahed, H.; Dubey, R. N. (1997): An axisymetric method for elastic-plastic analysis capable of predicting residual stress field. *Trans. ASME, J. Pressure Vessel Tech.*, vol. 119, pp. 264-273.

Kendall, D. P. (2000): A short history of high pressure technology from Bridgeman to Division 3. *Trans. ASME, J. Pressure Vessel Tech.*, vol. 122, pp. 229-233.

Levy, C.; Perl, M.; Kotagiri, S. (2006): The influence of the Bauschinger effect on 3-D stress intensity factors for internal longitudinal coplanar cracks in a fully or partially autofrettaged thick-walled cylinder. *Eng. Fracture Mech.,* vol. 73,

pp. 1814-1825.

Milligan, R. V.; Koo, W. H.; Davidson, T. E. (1966): The Bauschinger effect in a high strength steel. *Trans. ASME, J. Basic Eng.*, vol. 88, pp. 480-488.

Parker, A. P.; Farrow, J. R. (1980): On the equivalence of axisymmetric bending, thermal, and autofrettage residual stress fields. *J. Strain Anal.*, vol. 15, pp. 51-52.

Parker , A. P.; Underwood, J. H. (1998): Influence of the Bauschinger effect on residual stresses and fatigue lifetimes in autofrettaged thick-walled cylinders. *Fatigue and Fracture Mechanics, 29th Vol. ASTM STP 1321.* T. L. Panontin and S. D. Sheppard, eds., ASTM, PA.

Parker, A. P.; Underwood, J. H.; Kendall, D. P. (1999): Bauschinger effect design procedure for autofrettaged tubes including material removal and Sachs' method. *Trans. ASME, J. Pressure Vessel Tech*, vol. 121, pp. 430-437.

Parker, A. P. (2001): Autofrettage of open-end tubes – pressure, stresses, strains, and code comparison. *Trans. ASME, J. Pressure Vessel Tech.*, vol. 123, pp. 271-281.

Perl, M. (1988): The temperature field for simulating partial autofrettage in an elasto-plasic thick-walled cylinder. *Trans. ASME, J. Pressure Vessel Tech.*, vol. 110, pp. 100-102.

Perl, M.; Levy, C.; Wang, J. (1997): Interaction effects on the 3-D stress intensity factor of combined arrays of radial and longitudinal coplanar cracks in an internally pressurized thickwalled cylinder," *Trans. ASME, J.Pressure Vessel Tech.,* vol. 119, pp. 167-174.

Perl, M.; Greenberg, Y. (1999): Three dimensional analysis of thermal shock effect on inner semi-elliptical surface cracks in a cylindrical pressure vessel. *Int. J. Fracture*, vol. 99, pp. 163-172.

Perl, M.; Nachum A. (2000): 3-D stress intensity factors for internal cracks in an over-strained cylindrical pressure vessel, part I - the effect of autofrettage level. *Trans. ASME, J. Pressure Vessel Tech.*, vol. 122, pp. 421-426.

Perl, M.; Nachum A. (2001): 3-D Stress intensity factors for internal cracks in an over-strained

cylindrical pressure vessel, part II - the combined effect of pressure and autofrettage. *Trans. ASME, J. Pressure Vessel Tech.*, vol. 123, pp. 135-138.

Perl, M.; Levy, C.; Rallabhandy, V. (2006): Bauschinger effect's impact on the 3-D combined SIFs for radially cracked fully or partially autofrettaged thick-walled cylinders. *CMES: Computer Modeling in Engineering and Sciences: Special Issue on International Workshop on the Advancement of Computational Mechanics*, vol. 11, pp. 37-48.

Pu, S. L.; Hussain, M. A. (1983): Stress intensity factors for radial cracks in a partially autofrettaged thick-walled cylinder. *Fracture Mechanics: Fourteen Symposium-Vol. I: Theory and Analysis*, eds. J. C. Lewis and G. Sines, ASTM-STP 791, pp. I-194- I-215.

So, W. M. G.; Lau, K. J.; Ng, S. W. (2004): Determination of stress intensity factors for interfacial cracks using the virtual crack extension approach. *CMES: Computer Modeling in Engineering & Sciences,* vol. 5, pp. 189-200.

Nomenclature

a	crack depth
c	crack half length
d	distance between centers of two adjacent cracks
E	Young's Modulus
K_I	Mode I stress intensity factor (SIF)
K_{IA}	Mode I SIF due to autofrettage
K_{IP}	SIF due to pressurization
K_{IT}	SIF due to temperature field
K_{IN}	combined SIF $K_{IN} = K_{IP} - |K_{IA}|$
K_{Amax}	maximum K_{IA} along the crack front
K_{Pmax}	maximum K_{IP} along the crack front
K_{Nmax}	maximum K_{IN} along the crack front
K_{Ieff}	effective SIF $K_{Ieff} = K_{IP} + K_{IA} + K_{IT}$
K_0	reference SIF
N_f	fatigue life
n	number of cracks in the circumferential direction
n_P	Paris' exponent
p	internal pressure
r	radial coordinate
R_i	inner radius of the cylinder

R_o outer radius of the cylinder
t wall thickness of cylinder
x, y, z Cartesian coordinates

Greek Symbols

α coefficient of thermal expansion
ε level of autofrettage
ϕ parametric angle for elliptical cracks
θ angular coordinate
ν Poisson's ratio
σ_{yp} yield stress